

# Numerical Modelling of Sound Absorptive Properties of Double Porosity Granular Materials

Rodolfo Venegas<sup>\*1</sup> and Olga Umnova<sup>1</sup>

<sup>1</sup>Acoustics Research Centre, University of Salford, UK.

\*Newton Building, University of Salford, Salford, UK. M5 4WT, r.g.venegascastillo@edu.salford.ac.uk

**Abstract:** Granular materials have been conventionally used for acoustic treatment due to their sound absorptive and sound insulating characteristics. An emerging field is the study of acoustical properties of multi-scale porous materials. An example of these is a double-porosity granular material in which the grains are porous themselves. In this work, a computational methodology for modelling this type of material is presented. It is based on the homogenization of periodic media technique and accounts for rarefaction effects under non-isothermal sound propagation condition at the microscopic level. It is concluded that a double-porosity granular material exhibits reduced weight, remarkable low-frequency sound absorption enhancement and higher transmission loss for a given frequency range compared to its single-porosity counterpart.

**Keywords:** granular materials, double porosity, rarefaction effects, sound absorption, transmission loss.

## 1. Introduction

Acoustics of porous media is a very diverse subject which requires the knowledge of different branches of physics such as fluid dynamics and heat transfer theory<sup>1</sup>. Its applications can be found in a wide range of areas such as building and room acoustics, automotive and aerospace industries, oil exploration and marine sediments among others. Traditionally, materials with single pore size or a narrow grain/pore size distribution, i.e. single-porosity materials, have been considered for acoustic treatment<sup>1</sup>. Currently, the models that rely on macroscopic independently measured parameters are well-established and widely used to describe the acoustic behaviour of these materials<sup>1-5</sup>. A clear understanding of the microstructure influence on the macroscopic acoustical properties is however still elusive. The homogenization of periodic media theory (HPM) has provided a theoretical framework to study

this micro-macro relation<sup>6-7</sup>. The influence of granular materials microstructure on their acoustical properties has been studied in several recent publications. For example, Gasser et al.<sup>8</sup> predicted the acoustic and mechanical behaviour of nickel hollow spheres arranged in a face-centred cubic packing. A similar work has been published by Lee et al.<sup>9</sup> for simple cubic (SC), body-centred cubic (BCC), face-centred cubic and hexagonal close-packed configurations.

An emerging field is the study of the acoustical properties of multi-scale porous materials<sup>10</sup>. These materials have pores with two or more distinctively different sizes and can provide effective acoustic treatment at low-frequencies. Low frequency sound attenuation by a thin layer of a light-weight material is a long-standing problem in acoustic engineering. The existing theory has been applied to model meso-perforated porous materials<sup>10</sup>. However, so far it has not been applied to double-porosity materials with different morphology. Moreover, this theory does not consider the influence of rarefaction effects at the microscopic level. In this work, a numerical procedure for modelling double porosity granular materials is presented. The influence of rarefaction effects in the micropores is taking into account assuming non-isothermal sound propagation. The theory and governing equations are presented in Section 2. Following this, Section 3 presents the results and discussion. Conclusions are provided in Section 4.

## 2. Theory and governing equations

Three scales are used to describe the acoustic behaviour in a double porosity granular material. Figure 1 shows a schematic representation of these scales. The macroscopic characteristic size  $L$  is associated with the wavelength  $\lambda$  in the material as<sup>10</sup>  $L = O(|\lambda / 2\pi|)$ . The mesoscopic characteristic size  $l_p$  is determined by the size of the meso-heterogeneities, which in this case corresponds to the grain size. The microscopic

characteristic size  $l_m$  is determined by the size of the pores in the grains. To model the material as a homogenous equivalent fluid, the separation of scales among all the involved characteristic sizes should be satisfied. This is quantified through the inter-scale ratios  $\varepsilon = l_p / L \ll 1$  and  $\varepsilon_0 = l_m / l_p \ll 1$ . The existence of the representative elementary volumes REV<sub>m</sub>  $\Omega_m$  and REV<sub>p</sub>  $\Omega_p$  can then be ensured provided that these conditions on the inter-scale ratios are fulfilled. The meso and micro scales have associated porosities  $\phi_p = \Omega_{fp} / \Omega_p$  and  $\phi_m = \Omega_{fm} / \Omega_m$  with  $\Omega_{fi}$  being the voids/pore volume and  $\Omega_i$  the volume of the REV's. The subscript  $i$  takes values  $i = p, m$  henceforth. The overall porosity of the material is  $\phi_{db} = \phi_p + (1 - \phi_p) \phi_m$ .

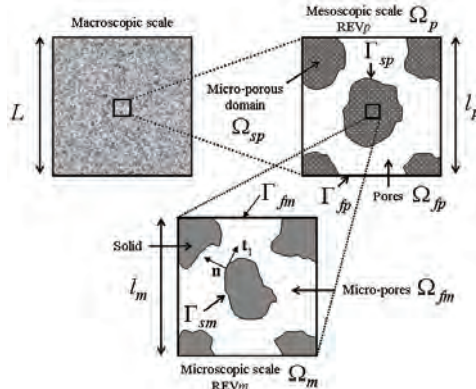


**Figure 1.** Three scales of a double porosity medium (adapted from Ref.<sup>10</sup>).

The application of the homogenization for periodic media theory to the deduction of the wave equation in a double porosity material including rarefactions effects at the microscopic level is rather lengthy and therefore presented elsewhere<sup>11</sup>. It closely follows the development presented by Olny and Boutin<sup>10</sup> but the non-slip and isothermal boundary conditions on  $\Gamma_{sm}$  are replaced by the slip and temperature-jump boundary conditions respectively. When the characteristic pore size becomes comparable to the mean free path, the porous medium cannot accommodate a large enough number of gas molecules. The saturating fluid may not therefore be assumed to have matter continuously distributed throughout the space it occupies<sup>11-15</sup>. The abovementioned boundary conditions modify the continuum description, which allows

accounting for rarefaction effects<sup>11-15</sup>. A measure of the degree of rarefaction is the Knudsen number. It is defined as  $K_n = l_{mean} / l_m$  with the mean free path given by  $l_{mean} = \eta \sqrt{\pi R_g T} / p$  where  $R_g$  is the specific gas constant and  $T$  and  $p$  are the temperature and pressure of the gas. For air at normal conditions  $l_{mean} \approx 60\text{nm}$ . Although the modified continuum description is valid only in the so-called slip-flow regime ( $0.01 < K_n < 0.1$ ), comparisons with measurements have shown good agreement for Knudsen number values even greater than one<sup>12</sup>.

The wave equation in a rigid double-porosity material<sup>10-11</sup> saturated by a Newtonian fluid is given by Eq. (1)

$$\frac{j\omega}{K_{db}(\omega, K_n)} p - \nabla \cdot \left( \frac{\mathbf{k}_{db}(\omega, K_n)}{\eta} \nabla p \right) = 0 \quad (1)$$

where  $p$  is the acoustic pressure in the equivalent fluid,  $\omega$  is the angular frequency and  $\eta$  is the dynamic viscosity of the saturating fluid. The dynamic bulk modulus and dynamic permeability of the double-porosity medium are denoted as  $K_{db}$  and  $\mathbf{k}_{db}$  respectively. The latter becomes a scalar quantity for isotropic media, i.e.  $\mathbf{k}_{db} = k_{db} \mathbf{I}$ , where  $\mathbf{I}$  is the unitary second-rank tensor. The way of calculating these two intrinsic quantities depends on the inter-scale ratio  $\varepsilon_0$ . The most interesting scenario is observed when  $\varepsilon_0 \approx 10^{-3}$ . This is usually referred to as high-permeability contrast<sup>10</sup>. In the context of this study, this case is seen when the grain and the micropore sizes are of the order of millimeters and micrometers respectively. Under this condition, the macroscopic flow is given by that of the mesoscopic pore network with the pores in the grains having no contribution<sup>10-11</sup>. The dynamic permeability is given by Eq. (2).

$$k_{db} = k_p(\omega) + (1 - \phi_p) k_m(\omega, K_n) \approx k_p(\omega) \quad (2)$$

where  $k_p$  and  $k_m$  are the dynamic permeabilities of the mesoscopic (as if the grains were solid) and the microscopic domains respectively.

The dynamic flow at the mesoscopic level is governed by an oscillatory Stokes forced problem with zero velocity (no-slip) condition on  $\Gamma_{sm}$  along with incompressibility condition<sup>7</sup>. This linear problem can be written in terms of the dynamic permeability field  $\hat{\mathbf{k}}_p$ . This makes

use of a local dynamic Darcy's law and the fact that the pressure can be expressed in terms of its deviatoric part and zero mean value<sup>7</sup>  $\hat{\pi}_p$ . The resulting problem is shown in Eq. (3) to (5).

$$j\omega(\rho_0/\eta)\hat{\mathbf{k}}_p + \nabla\hat{\pi}_p - \Delta\hat{\mathbf{k}}_p = \mathbf{I} \text{ in } \Omega_{fp} \quad (3)$$

$$\nabla \cdot \hat{\mathbf{k}}_p = 0 \text{ in } \Omega_{fp} \quad (4)$$

$$\hat{\mathbf{k}}_p = 0 \text{ on } \Gamma_{sp} \quad (\hat{\mathbf{k}}_p : \Omega_p\text{-periodic}) \quad (5)$$

where  $\rho_0$  is the density of the saturating fluid. The dynamic permeability of the mesoscopic domain is then obtained by averaging the solution over the REVp as follows<sup>7</sup>:

$$\mathbf{k}_p(\omega) = \langle \hat{\mathbf{k}}_p \rangle_p = \frac{1}{\Omega_p} \int_{\Omega_{fp}} \hat{\mathbf{k}}_p d\Omega \quad (6)$$

For isotropic media  $\mathbf{k}_p = k_p \mathbf{I}$ .

Following similar arguments, the dynamic fluid flow at the microscopic level is governed by the same set of equations as for the mesoscopic level but with slip boundary condition applied<sup>11-15</sup> on  $\Gamma_{sm}$ . This states that the velocity on the surface is proportional to the tangential shear stress<sup>14</sup>. This problem is also linear and can be written in terms of the microscopic dynamic permeability field<sup>14</sup>  $\hat{\mathbf{k}}_m$ . The canonical problem to be solved is given by Eq. (7) to (9).

$$j\omega(\rho_0/\eta)\hat{\mathbf{k}}_m + \nabla\hat{\pi}_m - \Delta\hat{\mathbf{k}}_m = \mathbf{I} \text{ in } \Omega_{fm} \quad (7)$$

$$\nabla \cdot \hat{\mathbf{k}}_m = 0 \text{ in } \Omega_{fm} \quad (\hat{\mathbf{k}}_m : \Omega_m\text{-periodic}) \quad (8)$$

$$\hat{\mathbf{k}}_m = -K_n(\mathbf{t}_1 \cdot \nabla \hat{\mathbf{k}}_m \cdot \mathbf{n})\mathbf{t}_1 \text{ on } \Gamma_{sm} \quad (9)$$

where  $\mathbf{n}$  is the normal vector to  $\Gamma_{sm}$  pointing outward from the pore region and  $\mathbf{t}_1$  is the tangential vector collinear with the wall slip<sup>14</sup> (see Figure 1). This formulation requires  $\varepsilon_0 \ll K_n \ll 1$ . The dynamic permeability is then calculated, in a first order approximation, by averaging the solution over the REVm<sup>11,14</sup>.

$$\mathbf{k}_m(\omega, K_n) = \langle \hat{\mathbf{k}}_m \rangle_m = \frac{1}{\Omega_m} \int_{\Omega_{fm}} \hat{\mathbf{k}}_m d\Omega \quad (10)$$

For isotropic media  $\mathbf{k}_m = k_m \mathbf{I}$ .

The dynamic bulk modulus for a double-porosity high-permeability contrast material<sup>10-11</sup> is given by Eq. (11).

$$\frac{1}{K_{db}} = \frac{1}{K_p(\omega)} + \frac{(1-\phi_p)F(\omega P_0 / \phi_m K_m(\omega, K_n), K_n)}{K_m(\omega, K_n)} \quad (11)$$

where  $K_p$  and  $K_m$  are the dynamic bulk modulus of the mesoscopic and microscopic

domain respectively. These can be calculated as function of the dynamic thermal permeabilities<sup>3,5</sup>  $k'_p$  and  $k'_m$  as is shown in Eq. (12).

$$K_i = (\gamma P_0 / \phi_i) \left( \gamma - j\omega \rho_0 (\gamma - 1) C_p k'_i(\omega, K_n) / \kappa \phi_i \right)^{-1} \quad (12)$$

where  $C_p$  is the specific heat at constant pressure,  $\kappa$  is the thermal conductivity,  $\gamma$  is the ratio between the specific heats and  $P_0$  is the static pressure.

The thermal exchanges between the saturating fluid and the solid matrix in the mesoscopic domain are governed by an oscillatory heat transfer problem with zero temperature<sup>3,5</sup> on  $\Gamma_{sp}$ .

This linear problem can be written in terms of the dynamic thermal permeability distribution  $\hat{k}'_p$  using a local analogous Darcy's thermal law<sup>3,5</sup>. The dynamic thermal permeability of the mesoscopic domain is calculated by averaging the solution of the canonical problem given by Eq. (13) and (14) over the REVp (Eq. (15)).

$$j\omega(\rho_0 C_p / \kappa) \hat{k}'_p - \Delta \hat{k}'_p = I \text{ in } \Omega_{fp} \quad (13)$$

$$\hat{k}'_p = 0 \text{ on } \Gamma_{sp} \quad (\hat{k}'_p : \Omega_p\text{-periodic}) \quad (14)$$

$$k'_p(\omega) = \langle \hat{k}'_p \rangle_p \quad (15)$$

At the microscopic level the thermal exchanges are also governed by an oscillatory heat transfer problem but with temperature-jump condition<sup>11-13,15</sup> applied on  $\Gamma_{sm}$ . This linear problem can be written in terms of the microscopic dynamic thermal permeability distribution<sup>11-13,15</sup>  $\hat{k}'_m$ . The dynamic thermal permeability of the microdomain is then calculated by averaging the solution of Eq. (16) and (17) over the REVm as is shown in Eq. (18).

$$j\omega(\rho_0 C_p / \kappa) \hat{k}'_m - \Delta \hat{k}'_m = I \text{ in } \Omega_{fm} \quad (16)$$

$$\hat{k}'_m = (2\gamma K_n / (\gamma + 1) N_{pr}) \nabla \hat{k}'_m \cdot \mathbf{n} \text{ on } \Gamma_{sm} \quad (17)$$

$$k'_m(\omega, K_n) = \langle \hat{k}'_m \rangle_m \quad (\hat{k}'_m : \Omega_m\text{-periodic}) \quad (18)$$

The function  $F$  in Eq. (11) is defined as the ratio of the average pressure in the microscopic domain to that in the mesoscopic domain<sup>10</sup>. It is related to the dynamic pressure diffusion function  $D(\omega, K_n)$  as follows<sup>10-11</sup>:

$$F(\omega, K_n) = 1 - j\omega(\phi_m \eta / P_0 (1 - \phi_p) k_{0m}) D(\omega, K_n) \quad (19)$$

where  $k_{0m} = k_{0m}(K_n)$  is the Knudsen number-dependent static viscous permeability of the

microdomain. The pressure in the microdomain is not uniform and is governed by a diffusion equation<sup>10</sup>. The boundary condition for this equation is imposed by the pressure in the mesoscopic domain which is both diffused into the microdomain and varies at the macroscopic scale<sup>10</sup>. This linear problem is written in terms of the mesoscopic dynamic  $\Omega_p$ -periodic pressure diffusion distribution  $\hat{D}$  in Eq. (20) and (21).  $D(\omega, K_n)$  is then calculated by averaging the solution over the solid phase of REVp.

$$\Delta \hat{D} - j\omega (\phi_m \eta / P_0 k_{0m}) \hat{D} = -I \text{ in } \Omega_{sp} \quad (20)$$

$$\hat{D} = 0 \text{ on } \Gamma_{sp} \quad (21)$$

$$D(\omega, K_n) = \langle \hat{D} \rangle = \frac{1}{\Omega_p} \int_{\Omega_{sp}} \hat{D} d\Omega \quad (22)$$

This completes the direct approach. All the quantities can be calculated from their definitions for every frequency of interest. This requires, however, a significant computational cost. To overcome this problem, one can use scaling functions that correctly match the low- and high-frequency asymptotic of the dynamic bulk moduli, permeabilities and pressure diffusion function<sup>2-5,10,11,15,16</sup>. In this way the acoustic description is reduced to solving three static problems per scale and one for the pressure diffusion function. This is detailed below.

The dynamic viscous permeabilities can be calculated using an extension of the model proposed by Pride et al.<sup>4</sup>. This model accounts for rarefaction effects<sup>15</sup>. Its expression is given by Eq. (23).

$$k_i(\omega, K_n) = k'_{0i} \left( \frac{j\omega}{\omega_{vi}} + 1 - P_{vi} + P_{vi} \sqrt{1 + \frac{j\omega}{\omega_{vi}} \left( \frac{M_{vi}}{2P_{vi}^2} \right)} \right)^{-1} \quad (23)$$

where  $P_{vi} = M_{vi} / 4(\alpha_{0i} / \alpha_{xi} - 1)$ ,  $M_{vi} = 8k_{0i}\alpha_{xi}/\phi_i\Lambda_i^2$  and the viscous characteristic frequency is defined as  $\omega_{vi} = \eta\phi_i/\alpha_{xi}k_{0i}\rho_0$ . The static viscous permeabilities  $k_{0p}$  and  $k_{0m}(K_n)$  are calculated by setting  $\omega = 0$  and solving Eq. (3) to (6) and Eq. (7) to (10) respectively. Using these solutions one can calculate the static viscous tortuosities as  $\alpha_{0i} = \phi_i \langle \hat{k}_{0i}^2 \rangle_i \langle \hat{k}_{0i} \rangle_i^{-2}$ . At high frequencies, viscosity effects can be neglected and the fluid flow satisfies the Laplace equation (potential flow)<sup>2</sup>. The same type of equation also describes the electrical conduction problem for a porous medium in which the solid phase is insulating

and the saturating fluid is conducting<sup>17</sup>. This problem is shown in Eq. (24) and (25).

$$\nabla^2 \vartheta_i = 0 \text{ in } \Omega_{fi} \quad (24)$$

$$\mathbf{n} \cdot \nabla \vartheta_i = \mathbf{n} \cdot \mathbf{e} \text{ on } \Gamma_{si} \quad (25)$$

where  $\vartheta_i$  is the  $\Omega_i$ -periodic deviatoric part of an electric potential. It is related to the scaled electric field (local electrical field divided by the applied macroscopic potential gradient) as  $\mathbf{E}_i = \mathbf{e} - \nabla \vartheta_i$  (Hodge decomposition) where  $\mathbf{e}$  is the unitary external electric field. For isotropic materials the tortuosities  $\alpha_{xp}$  and  $\alpha_{xm}$  and viscous characteristic lengths  $\Lambda_p$  and  $\Lambda_m$  are calculated using Eq. (26) and (27). These parameters do not depend on the Knudsen number<sup>12,13,15</sup>.

$$\phi_i \alpha_{xi}^{-1} = \langle \mathbf{E} \cdot \mathbf{e} \rangle_i \quad (26)$$

$$\Lambda_i = 2 \int_{\Omega_{fi}} \mathbf{E}_i \cdot \mathbf{E}_i d\Omega / \int_{\Gamma_{si}} \mathbf{E}_i \cdot \mathbf{E}_i d\Gamma \quad (27)$$

The dynamic thermal permeabilities including rarefaction effects can be calculated using an extension of the model<sup>15</sup> proposed by Lafarge<sup>5</sup> as is shown in Eq. (28).

$$k'_i(\omega, K_n) = k'_{0i} \left( \frac{j\omega}{\omega_{ii}} + 1 - P_{ii} + P_{ii} \sqrt{1 + \frac{j\omega}{\omega_{ii}} \left( \frac{M_{ii}}{2P_{ii}^2} \right)} \right)^{-1} \quad (28)$$

where  $P_{ii} = M_{ii} / 4(\alpha'_{0i} - 1)$ ,  $M_{ii} = 8k'_{0i}/\phi_i\Lambda_i'^2$  and the thermal characteristic frequencies are defined as  $\omega_{ii} = \kappa\phi_i/C_p\rho_0k'_{0i}$ . The static thermal permeabilities  $k'_{0p}$  and  $k'_{0m}$  can be calculated by setting  $\omega = 0$  in Eq. (13) to (15) and Eq. (16) to (18) respectively. The static thermal tortuosities are calculated as  $\alpha'_{0i} = \phi_i \langle \hat{k}_{0i}^{i2} \rangle_i \langle \hat{k}'_{0i} \rangle_i^{-2}$ . The thermal characteristic length is a geometrical parameter defined as twice the volume-to-pore-surface ratio<sup>1</sup>, i.e.  $\Lambda'_i = 2\Omega_{fi}/\Gamma_{si}$ .

The dynamic pressure diffusion function can also be calculated using a scaling function<sup>16</sup> which is given by Eq. (29).

$$D(\omega, K_n) = D_0 \left( \frac{j\omega}{\omega_d} + 1 - P_d + P_d \sqrt{1 + \frac{j\omega}{\omega_d} \left( \frac{M_d}{2P_d^2} \right)} \right)^{-1} \quad (29)$$

where  $P_d = M_d / 4(\alpha_d - 1)$ ,  $M_d = 8D_0 / (1 - \phi_p)\Lambda_d^2$  and the pressure diffusion characteristic frequency is defined as  $\omega_d = (1 - \phi_p)P_0 k_{0m} / \eta\phi_m D_0$ . The static pressure diffusion value<sup>10</sup> is calculated from Eq. (20) to (22) by setting  $\omega = 0$ . The static

pressure diffusion tortuosity<sup>16</sup> is defined as  $\alpha_d = (1 - \phi_p) \langle \hat{D}_0^2 \rangle \langle \hat{D}_0 \rangle^{-2}$ , The pressure diffusion characteristic length<sup>10</sup> is given by  $\Lambda_d = 2\Omega_{sp} / \Gamma_{sp}$ . The characteristic impedance  $Z_c^{db}(\omega, K_n)$  and the wave number  $k_c^{db}(\omega, K_n)$ , which provide all the necessary information to characterize sound propagation in a given medium<sup>1</sup>, are shown in Eq.(30).

$$k_c^{db} = \omega \sqrt{\rho_{db} K_{db}^{-1}} \text{ and } Z_c^{db} = \sqrt{\rho_{db} K_{db}} \quad (30)$$

The surface impedance  $Z_w^{db}$  of a rigidly-backed layer of a material of thickness  $q$  is given by Eq. (31) whilst the reflection  $R_{db}$  and absorption  $\alpha_{db}$  coefficients by Eq. (32). The sound transmission loss<sup>1</sup> of a layer of thickness  $q$  loaded at both sides by a fluid with characteristic impedance  $Z_0 = \rho_0 c_0 = \rho_0 \sqrt{\gamma P_0 / \rho_0}$  can be estimated from the entries of its transfer matrix<sup>1</sup>. The expression for its calculation is shown in Eq. (33).

$$Z_w^{db} = -j Z_c^{db} \cot(k_c^{db} q) \quad (31)$$

$$R_{db} = (Z_w^{db} - Z_0)(Z_w^{db} + Z_0)^{-1} \text{ and } \alpha_{db} = 1 - |R_{db}|^2 \quad (32)$$

$$\frac{TL}{20} = \log \left| \cos(k_c^{db} q) + j \sin(k_c^{db} d) \left( \frac{(Z_c^{db})^2 + Z_0^2}{2Z_0 Z_c^{db}} \right) \right| \quad (33)$$

### 3. Results

Two different granular packings have been considered as mesoscopic geometry. The first one corresponds to the body-centred cubic BCC close packing whilst the second one to a simple-cubic packing SC. These serve as model for unconsolidated and consolidated granular materials respectively. In both cases, the mesoporosity is set to  $\phi_p = 0.32$ . The particle radius equals to  $r_p = 0.5$  mm. All the canonical problems presented in the foregoing section have been solved using COMSOL® Multiphysics. Figure 2 shows the principal component of the normalized static viscous permeability field  $\hat{k}_{0,p}$  (left) and the static thermal permeability distribution  $\hat{k}'_{0,p}$  (right) for BCC (top) and SC (bottom). These have been mapped to the interval [-1, 1] considering their minimum and maximum values throughout the REVp. The

macroscopic parameters calculated by averaging the solution of the static problems are shown in Table 1. The inner structure of the grains is assumed to be a staggered array of circular micropores, referred to as CP henceforth, of radius  $r_m$  and microporosity  $\phi_m$ . The macroscopic parameters of CP have been numerically calculated and compared to the following analytical solutions<sup>12</sup>.  $k_{0m}(K_n) / \phi_m = r_m^2 (1 + 4K_n) / 8$ ;  $\Lambda_m = \Lambda'_m = \alpha_\infty = 1$  and  $k'_{0m} = k_{0m} (2\gamma\kappa K_n / (\gamma+1)C_p\eta)$ . The static tortuosities are introduced here and given by  $\alpha_{0m}(K_n) = (4/3)(1 + 6K_n(2K_n + 1)) / (1 + 4K_n)^2$  and  $\alpha'_{0m} = \alpha_{0m} (2\gamma\kappa K_n / (\gamma+1)C_p\eta)$ . An excellent agreement (maximum error of 0.17%) has been obtained over the whole range of valid Knudsen numbers for all of these parameters.

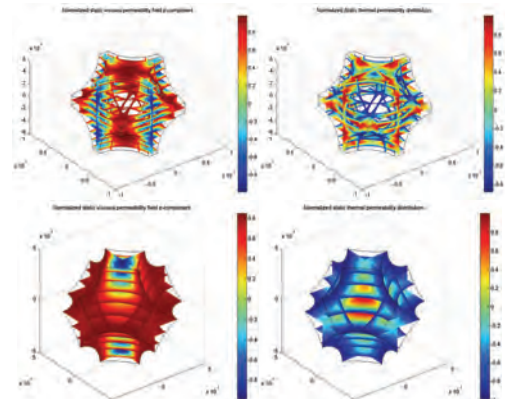


**Figure 2.** Normalized principal component of the static viscous permeability field (left) and static thermal permeability distribution (right) for BCC (top) and SC (bottom) packing.

**Table 1:** Macroparameters for BCC and SC

	$k_0 / r^2 \cdot 10^{-3}$	$\alpha_0$	$k'_0 / r^2 \cdot 10^{-3}$	$\alpha'_0$
BCC	2.005	1.8661	3.927	1.3513
SC	2.652	2.4511	8.693	1.4939
	$\Lambda / r$	$\Lambda' / r$	$\alpha_\infty$	$\phi$
BCC	0.1867	0.3137	1.4721	0.32
SC	0.2877	0.4227	1.7368	0.32

Figure 3 shows the real (blue) and imaginary (red) parts of the scaled dynamic pressure diffusion function. The numerical solution of the dynamic problem (Eq. (22)) for a discrete set of frequencies is shown with circles. Continuous

line corresponds to the model<sup>16</sup> given by Eq (29). The inset plots show the normalized static pressure function distribution  $\hat{D}_0$  (left) and the absolute value of the normalized principal component of the viscous permeability field  $\hat{k}_{0m}$  (right). For this simulation, the micropore radius has been set to  $r_m = 0.6 \mu\text{m}$  ( $K_n = 0.1$ ) and the microporosity to  $\phi_m = 0.6$ . The pressure diffusion macroscopic parameters take values  $D_0 / r_p^2 = 0.05779$ ,  $\Lambda_d / r_p = 0.6489$  and  $\alpha_d = 1.3118$ . The model is in excellent agreement with the simulation of the dynamic problem.

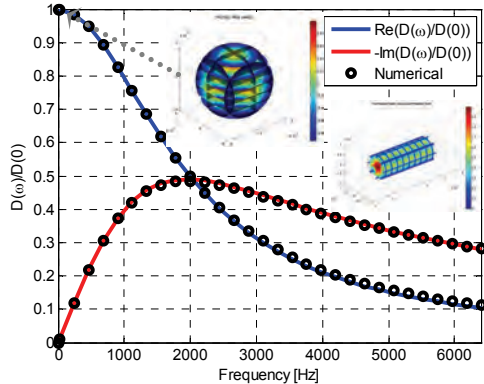


**Figure 3.** Scaled dynamic pressure diffusion function for a double-porosity SC-CP granular material. See the text for the inset plots.

Figure 4 shows the sound absorption coefficient of a 3-cm, rigidly-backed layer of a double-porosity BCC-CP granular material for different values of microporosity. The Knudsen number is  $K_n = 0.1$ . The numerically calculated static pressure diffusion parameters for BCC-CP are indistinguishable from the analytical solutions  $D_0 / r_p^2 = (1 - \phi_p) / 15$ ;  $\Lambda_d / r_p = 2 / 3$  and  $\alpha_d = 10 / 7$ .

As the microporosity increases, the sound absorption curve is largely shifted towards lower frequencies compared to the solid-grain case (blue dashed line). For example, the sound absorption coefficient at 500 Hz is 0.09 for BCC whilst is 0.36 for BCC-CP ( $K_n = 0.1, \phi_m = 0.6$ ). This improvement is accompanied by a weight reduction of  $100\phi_m = 60\%$ . This trend is also observed for a consolidated material SC-CP. Figure 5 shows sound absorption coefficient of a 3-cm, rigidly-backed layer of SC-CP for different Knudsen number values and

microporosity  $\phi_m = 0.6$ . The sound absorption curve of SC-CP is also shifted towards lower frequencies. It is seen that the smaller the micropore size the slightly better the low-frequency sound absorption is. However, the first absorptive peak is located at higher frequencies with respect to that of a material with larger micropores when keeping the microporosity constant.

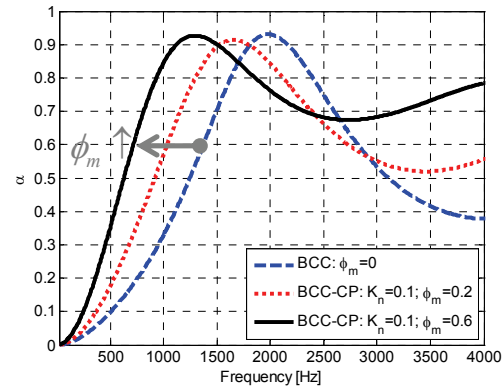


**Figure 4.** Sound absorption coefficient of BCC-CP for different microporosity values.

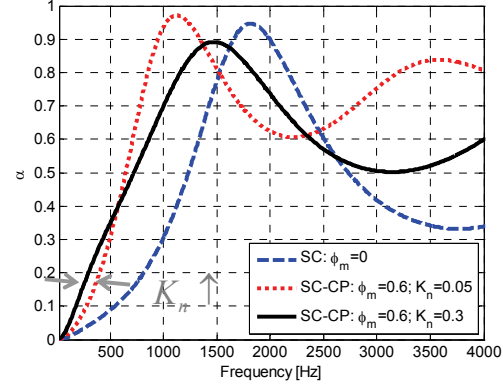


**Figure 5.** Sound absorption coefficient of SC-CP for different Knudsen number values.

Figure 6 shows the transmission loss of a 3-cm layer of BCC-CP for different Knudsen numbers and microporosity values. Increasing the microporosity results in a larger high-frequency TL with respect to that of the solid-grain case. The low-frequency TL of BCC-CP increases when the micropore size is decreased. This however can be either slightly larger or slightly smaller (less than 1 dB on average) than that of BCC depending on the micropore size for a given microporosity value. The same trend is

observed for a consolidated SC-CP material. Taking into account that the weight is reduced by  $100\phi_m\%$ , this TL enhancement is encouraging and somewhat counterintuitive as the usual acoustic engineering rule for sound transmission loss is the *heavier* the material the *better* the sound insulation.

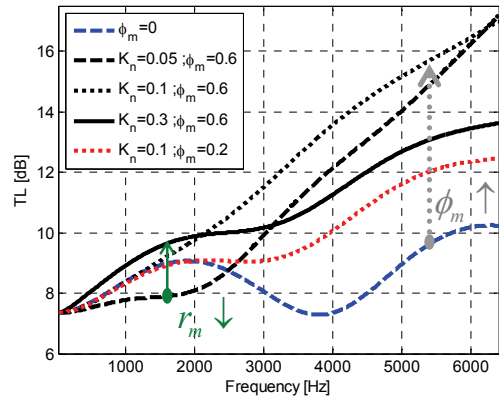


Figure 6. Transmission loss of BCC-CP for different microporosity and Knudsen number values.

#### 4. Conclusions

A numerical procedure for modeling double-porosity consolidated and unconsolidated granular materials has been presented. The results indicate that these materials present reduced weight, remarkable low-frequency sound absorption enhancement, similar low-frequency transmission loss and greater transmission loss at high frequencies compared to their single-porosity counterpart. This research presents new alternative approaches to acoustic treatment with naturally occurring or engineered materials.

#### 5. References

- J. F. Allard & N. Atalla. Propagation of Sound in Porous Media: Modeling Sound Absorbing Materials. John Wiley & Sons, 2009.
- D. L. Johnson, J. Koplik & R. Dashen, Theory of dynamic permeability and tortuosity in fluid-saturated porous media, *J. Fluid Mech.* **176**, pp. 379-402, 1987.
- D. Lafarge, P. Lemarinier, J.F. Allard & V. Tarnow, Dynamic compressibility of air in porous structures at audible frequencies, *J. Acoust. Soc. Am.* **102** (4), pp. 1995-2006, 1997.
- S. R. Pride, F. D. Morgan & A.F. Gangi, Drag forces of porous-medium acoustics, *Phys. Rev. B* **47**, pp. 4964-4975, 1993.
- D. Lafarge, Propagation du son dans les matériaux poreux à structure rigide saturés par un fluide viscothermique, Ph. D. Thesis, Université du Maine, 1993.
- E. Sanchez-Palencia, Nonhomogeneous Media and Vibration theory, Springer Verlag, 1980.
- J.-L. Auriault, L. Borne & R. Chambon, Dynamics of porous saturated media, checking of the generalized law of Darcy. *J. Acoust. Soc. Am.*, **77** (5), pp. 1641-1650, 1985.
- S. Gasser, F. Paun & Y. Brechet, Absorptive properties of rigid porous media: Application to face centered cubic sphere packing, *J. Acoust. Soc. Am.*, **117**(4), pp. 2090-2099, 2005.
- C-Y. Lee, M.J. Leamy & J.H. Nadler, Acoustic absorption calculation in irreducible porous media: A unified computational approach, *J. Acoust. Soc. Am.*, **126**(4), 2009.
- X. Olny & C. Boutin, Acoustic wave propagation in double porosity media, *J. Acoust. Soc. Am.*, **114**(1), 2003.
- R. Venegas & O. Umnova, paper to be submitted, 2010.
- V.F. Kozlov, A.V. Fedorov & N.D. Malmuth, Acoustic properties of rarefied gases inside pores of simple geometries, *J. Acoust. Soc. Am.* **117**, pp. 3402-3411, 2005.
- O. Umnova, D. Tsiklauri & R. Venegas, Effect of boundary slip on the acoustical properties of microfibrous materials, *J. Acoust. Soc. Am.*, **126**(4), pp.1850-1861, 2009.
- J. Chastanet, P.Royer & J.-L. Auriault, Acoustics with wall-slip flow of gas saturated porous media. Mechanics Research Communications, **31**, pp. 277-286, 2004.
- R. Venegas & O. Umnova, Effective acoustical properties of random microfibrous materials. *Proc.of Euronoise 2009*, Oct 26-28, 2009, Edinburgh, UK.
- R. Venegas, paper to be submitted, 2010.
- R. J. S. Brown, Connection between formation factor for electrical-resistivity and fluid-solid coupling factor in Biot equations for acoustic waves in fluid-filled porous media, *Geophysics*, **45**, pp. 1269–1275, 1980.

#### 6. Acknowledgements

R. Venegas gratefully acknowledges an ORSAS award and The University of Salford Research Studentship.